ACS Macro Letters

Letter

pubs.acs.org/macroletters

Assembly of Chitin Nanofibers into Porous Biomimetic Structures via Freeze Drying

Jie Wu[†] and J. Carson Meredith*[,‡]

[†]School of Materials Science and Engineering and [‡]School of Chemical and Biomolecular Engineering, Georgia Institute of Technology, Atlanta, Georgia 30332, United States

Supporting Information

ABSTRACT: The intricate hierarchical architectures in natural creatures are usually derived from assembly of molecular building blocks into nanoscale structures that then organize into micro- and macroscopic sizes. An example is the complex structure in arthropods (crustaceans, insects) constructed primarily of chitin. Because of chitin's inherent insolubility in common solvents, processes for mimicking the fascinating natural chitin-based nanostructures are still at an early stage of development. Here, we present a facile freeze-drying approach to assemble chitin nanofibers (20 nm diameter) into a variety of structures whose size and morphology are tunable by adjusting freezing temperature and heat transfer characteristics. We show that reducing the freezing rate allows controllable formation of structures ranging from oriented sheets to three-dimensional aperiodic nanofiber networks that mimic the size and interconnectivity of the white *Cyphochilus* beetle cuticle. The formation of nanofibrous structures is not predicted by the widely used particle encapsulation model of freeze-drying. We reason that this structure occurs due to a combination of attractive interactions of the nanofibers and a slow freezing rate that encapsulates and preserves the network structure. The method outlined here is likely applicable to creating fine nanofibrous structures with other polymers and materials classes with size ranges useful in diverse applications such as tissue engineering, filtration, and energy storage.

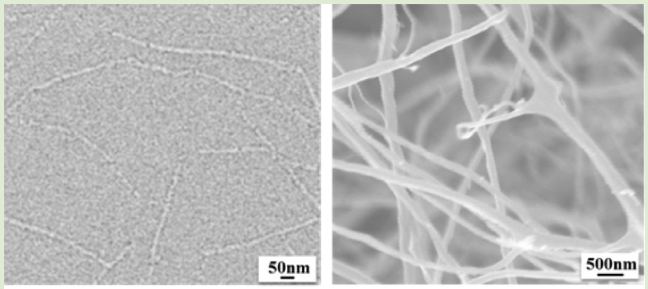

Chitin is a renewable and biodegradable polymer that assembles into crystalline nanofibers that are utilized by animals (arthropods) and fungi through organization into many sophisticated hierarchical structures. Being the second-most abundant naturally produced biopolymer (second to cellulose), 10^{10} to 10^{11} tons of chitin is produced each year in nature. However, chitin biomimicry remains a significant and unsolved challenge.[1−3] Chitin-based structures include the high-stiffness twisted plywood structure of lobster shells.[4] Another example is the *Cyphochilus* "white" beetle, which has unique whiteness arising from the chitin-rich three-dimensional aperiodic network structure within its cuticle.[5] This kind of porous nanofibrous structure is significant to a wide range of practical applications, including white paints and coatings, tissue engineering, catalysis, sensors, filtration, absorbents, actuators, structural materials, and energy storage (supercapacitors and batteries).[6−15] Constructed primarily of chitin and some protein, the white beetle cuticle is a model for mimicry to produce such porous nanofibrous materials from a renewable resource.

However, owing to its insolubility in common solvents and strong molecular interactions, chitin is challenging to process into controlled nanostructures.[1−3] Previously, man-made processes have not been reported to use chitin directly to reproduce the intricate cuticle structure. While self-assembly and electrospinning are potential candidates, they have not been demonstrated on chitin nanofibers directly, but rather they often require structure-directing additives (self-assembly) or depolymerization and use toxic or volatile organic solvents (electrospinning). These alterations detract from the sustainable nature of chitin.[16−18] Often, chitin is deacetylated to form chitosan, which is soluble in dilute acidic solutions. The processing of chitosan into nanostructured materials has been the subject of numerous investigations.[1,2,19,20] In contrast, we seek a method to assemble extracted chitin directly into nanofibrous structures with controlled size and interconnectivity, without any other additives or pretreatments that alter the polymer structure.

Freeze-drying has attracted intense interest as a general route to fabricate porous materials for a wide range of applications. Starting with a solution, emulsion, or dispersion, freezing causes solute or solids to be excluded by an advancing ice front into the interstitial spaces between ice crystals. Subsequent sublimation leads to porous structures. By controlling concentration and freezing direction, complex hierarchical morphologies are produced, including well-aligned channels, honeycombs, and brick-mortar-bridges.[21−27] Most studies focus

Received: October 25, 2013
Accepted: January 20, 2014
Published: January 28, 2014

   dx.doi.org/10.1021/mz400543f | *ACS Macro Lett.* 2014, 3, 185−190

on directional freezing under liquid nitrogen, but nondirectional, aperiodic nanofibrous structures similar to that of the white beetle have not been achieved by freeze-drying. In this letter, we demonstrate that adjusting variables expected to control freezing rate (freezing temperature or heat transfer characteristics) allows tuning the *dimensions and connectivity* of the chitin structures formed from an aqueous chitin nanofiber (CNF) dispersion. Depending on freezing conditions this method allows a broad variety of structures to be formed from chitin, from nanofibrous networks that mimic the white beetle to micrometer-scale oriented and random sheets. The general principle of reducing ice growth rate to achieve finer control of porous network structures, applied here to chitin, is likely applicable to other polymer and materials classes to produce structures of relevance to many practical applications, as noted above.[6−15]

CNFs were fabricated via fibrillation of purified chitin by high shear homogenization, as described in the experimental section of the Supporting Information. After homogenization, the CNF dispersion exhibits high optical transparency, and CNF has a zeta potential of +57.5 mV at pH 4.1, which originates from protonated $-NH_3^+$ groups and stabilizes the dispersion via electrostatic repulsion. Figure 1a and Figure S1 (Supporting Information) illustrate that single CNFs are present in water with an average diameter (d_{avg}) of 20 nm distributed over a range of 5−50 nm and lengths that vary between ∼100 nm and several micrometers. When allowed to dry at room temperature, the CNF dispersion forms an optically transparent film that is composed of relatively densely packed nanofibers (Figure 1b and 1c). Dense structures like these are typically formed when fibrous materials are dried from water under ambient conditions, due to compaction and adhesion of fibers that occur as solids concentration increases and additionally due to pore shrinkage in the late stages of drying due to the high surface tension of water.

All freeze-dried structures were produced at −20 °C, −80 °C, and −196 °C (liquid N_2), using a CNF aqueous suspension. The freeze-dried chitin prepared at −20 °C freezing temperature is white and opaque (Figure 2a) and consists of a three-dimensional aperiodic fibrous network structure with d_{avg} = 220 nm, ranging from 150 to 350 nm based on top, bottom, and cross-sectional SEM images (Figure 2b−e). These results show that single CNFs assemble into larger, randomly oriented interconnected fibril bundles during freezing, very similar to the white beetle scale structure (fibrous network structure with fiber diameter of around 250 nm).[5] While the fiber size and interconnectivity of freeze-dried chitin are similar to the white beetle structure, the synthetic structures are much more porous (>90% in Table 1) than the beetle structure (∼30%) (pore size distribution listed in Figure 2f). CNF suspensions were also frozen at −80 °C and −196 °C (liquid nitrogen), but these conditions do not produce fibrous structures. At −80 °C, the frozen chitin has a random porous architecture (Figure 3a and 3b) consisting of sheetlike structures, while parallel-walled structures result from liquid nitrogen freezing (Figure 3d). Oriented and sheet-like porous structures, similar to those derived here at −80 °C and −196 °C, have been reported before by utilizing different starting materials, and their structure formation mechanism has already been established.[22−24,28] Reports of freeze-drying chitosan (not chitin) at high temperature (−20 °C) have demonstrated macroporous sheet-like structures[19,20] but not fine nanofibrous structures created herein with chitin. As discussed below, we propose that the solubility of chitosan likely leads to precipitation into large domains during freezing, whereas starting with insoluble chitin nanofibers leads to a preservation of the nanoscale features.

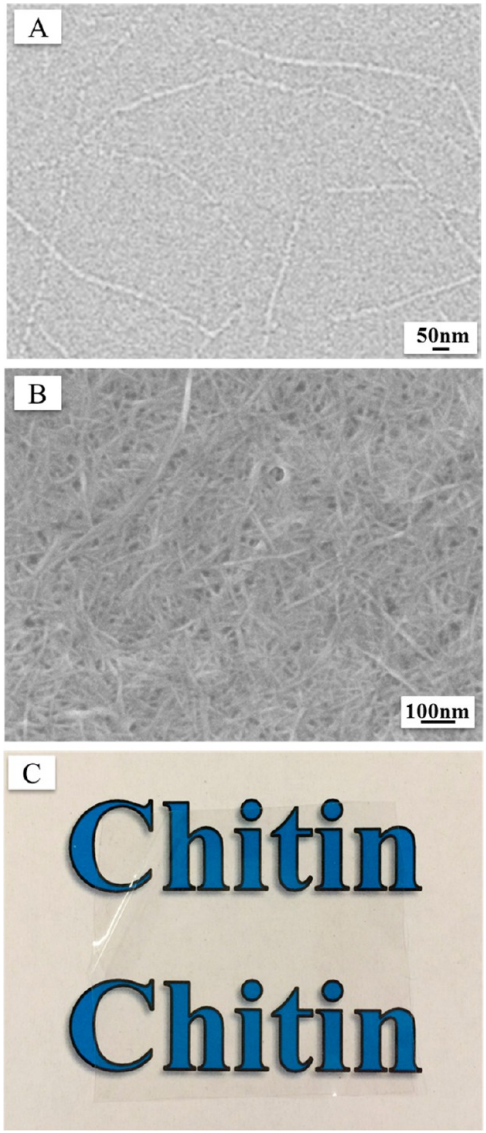

Figure 1. (a) SEM image of chitin nanofiber fabricated via fibrillation of purified chitin by high shear homogenization; (b) SEM image, and (c) photo of chitin nanofiber film produced by drying a chitin nanofiber/water dispersion at room temperature. The film is sitting on a printed background to illustrate its transparency.

Ice crystallization is well-characterized and consists of two successive processes: crystal nucleation and growth. The rate of ice nucleation is determined by the degree of supercooling, whereas the ice growth rate is largely controlled by the rate of heat transfer from the crystal surface to the bulk water.[29−31] A suspended particle close to an advancing ice front is acted on by two opposing forces: a repulsive force derived from van der Waals forces and an attractive force owing to viscous drag. A balance of these two forces yields a critical ice growth velocity at which particle encapsulation by the ice occurs. Below this velocity, particles repelled by ice should be pushed together into the interstitial spaces between ice crystals; e.g., formed structures are larger than the original particles. Above this critical velocity, the structures are encapsulated as ice grows

dx.doi.org/10.1021/mz400543f | ACS Macro Lett. 2014, 3, 185−190

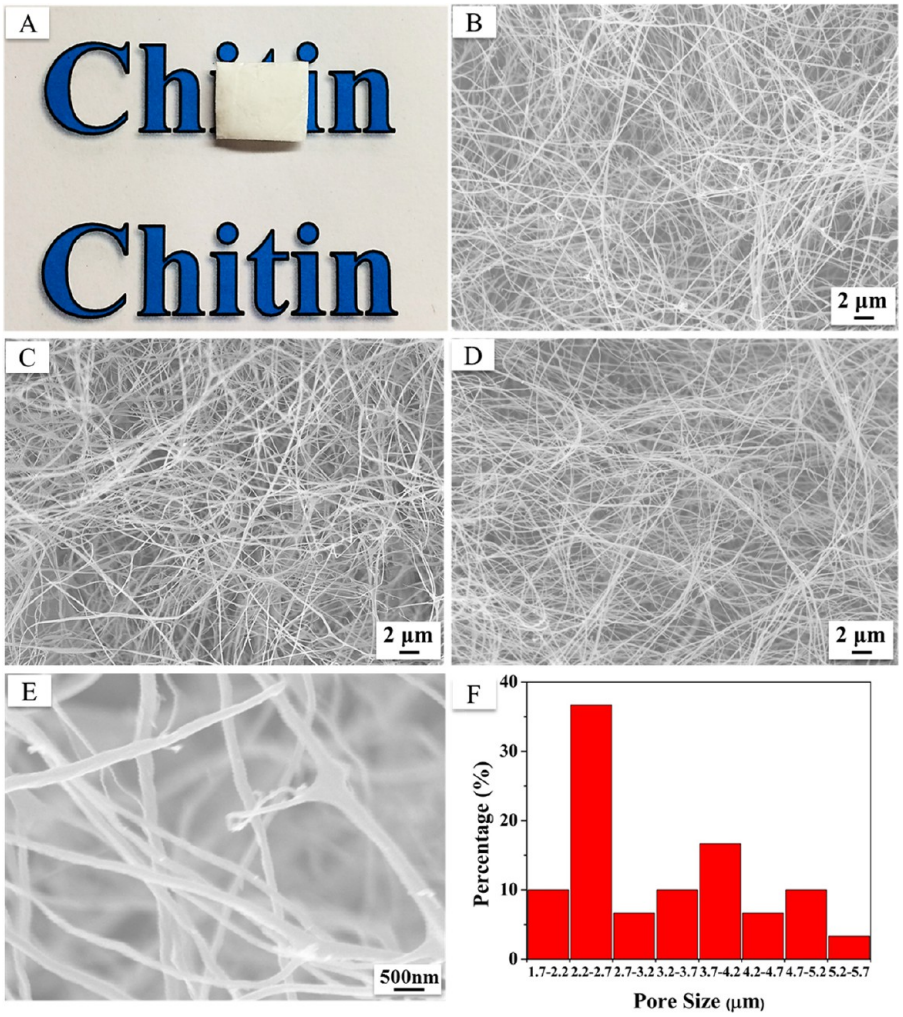

Figure 2. (a) Photo, (b) top, (c) bottom, (d) cross section, (e) enlarged top SEM images and (f) pore size distribution of freeze-dried chitin produced under −20 °C freezing (aluminum dish).

Table 1. Pore Size and Porosity of Freeze-Dried Chitin

temperature (°C)	mold	pore size (μm)	porosity (%)
−20	aluminum	3.2 ± 0.4	98.5
−80	aluminum	96 ± 12	99.5
−196	aluminum	59 ± 7.6	99.5
−20	stainless steel	0.33 ± 0.05	99.6

around the particles.[24,32,33] The formation of large (>10 μm) porous structures at −80 °C and −196 °C (Figure 3e and 3f), starting with 20 nm CNFs, indicates that ice front velocity was below the critical encapsulation velocity. At −196 °C, the CNF suspension is subject to a significant temperature gradient in the thickness direction, leading to fast ice crystallization in this direction to the orthogonal, leading to oriented porous structures (Figure 3c and 3d). Under −80 °C freezing, there was no preferred growth direction, likely due to the reduced temperature gradient, and CNFs were expelled by ice fronts to form large, disoriented sheet-like structures.

Ice growth rate should be slower at −20 °C than at −80 °C or −196 °C based on the reduced driving force for heat removal.[30,34] Thus, the ice growth velocity at −20 °C will be even further below the critical velocity for encapsulation of CNFs than at −80 °C. Hence, we expect that ice crystal size at −20 °C should be larger than that at −80 °C because slower freezing rate generally results in larger ice crystals.[26,31,35,36] However, the pore size of freeze-dried chitin observed from Figure 2b−e and Figure 3a,b is *smaller* at −20 °C than at −80 °C (pore size distribution shown in Table 1 and Figures 2f and 3e), which indicates that they are not controlled by ice crystal size. This implies that CNFs are encapsulated and are not pushed to interstitial boundaries. Hence, the observation of smaller pore size at −20 °C contradicts the prediction of the particle encapsulation model. We suggest that this discrepancy is due to the fact that CNFs do not behave as independent particles but experience significant interactions. For example, chitin nanocrystals exhibit strong van der Waals attraction and electrostatic interactions and are known to form nematic gels with increasing concentration in water.[37]

The proposed mechanism for formation of fibrous network structures under −20 °C freezing is illustrated in Figure 4. First, CNFs are well dispersed in water at pH 4 due to strong electrostatic repulsion. When the CNF suspension is supercooled sufficiently, ice starts to nucleate and grow. Initially, isolated CNFs are pushed together by the advancing ice fronts, leading to fiber−fiber interactions such as van der Waals attraction, electrostatic repulsion, and hydrogen bonding. At this stage we propose that individual CNFs assemble into interconnected nanofiber bundles between 150 and 350 nm in diameter. As ice continues to grow slowly, these bundles do not

dx.doi.org/10.1021/mz400543f | ACS Macro Lett. 2014, 3, 185−190

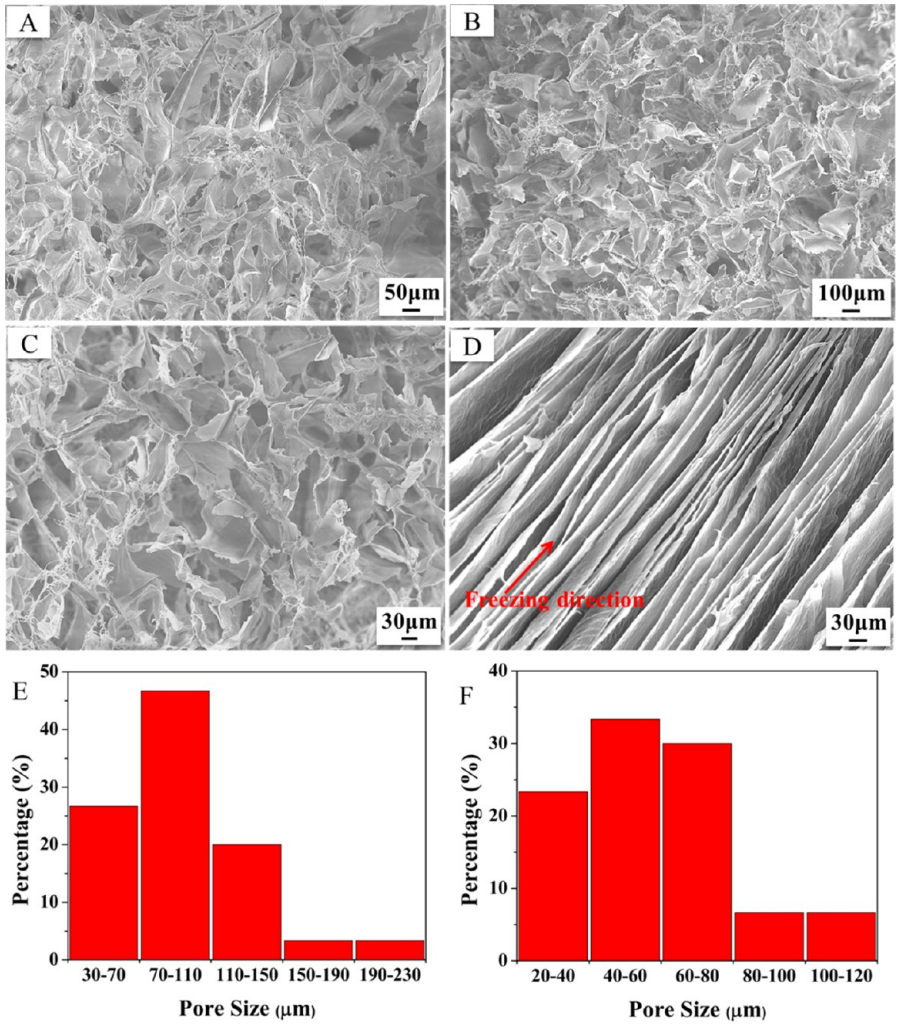

Figure 3. SEM images of freeze-dried chitin: (a) top and (b) cross section of sample produced at −80 °C freezing and (c) top and (d) cross section of sample produced under liquid nitrogen freezing. Pore size distributions of freeze-dried chitin: (e) −80 °C freezing and (f) liquid nitrogen freezing.

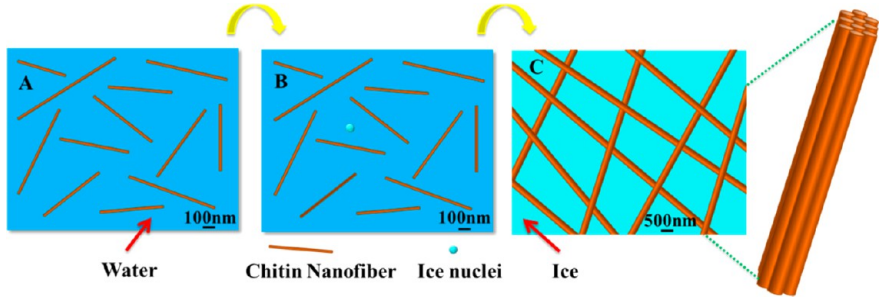

Figure 4. Schematic representation of assembly of chitin nanofibers under −20 °C freezing: (a) chitin nanofiber/water dispersion; (b) advent of ice nuclei; and (c) chitin nanofiber bundles encapsulated in ice.

become oriented but rather form a three-dimensional aperiodic network structure with fiber diameters averaging about 220 nm. This network structure can apparently resist being broken by the advancing ice fronts, and the growing ice crystals pass around and encapsulate this network instead. Since the ice growth rate is expected to be relatively slower at −20 °C than at −80 °C, we argue that single CNFs have more time to reorient and align into packed bundles at −20 °C, whereas the advancing ice front more quickly expels CNFs and then ruptures the developed network structure under −80 °C and −196 °C freezing to form sheet-like structures (faster aggregation). A previous report showed that chitosan dissolved in acetic acid formed large macroporous sheet structures under −20 °C freezing.[20] Because chitosan was dissolved, fibers were not initially present to form a network in the early stages of freezing. Rather, the chitosan formed phase-separated micrometer-sized structures as solution concentration increased in the interstitial spaces. Hence, formation of the fine network structure likely depends on the initial presence of fine insoluble chitin fibers.

Above, we have shown that tuning freezing temperature results in adjustable pore structure and have argued that this is

dx.doi.org/10.1021/mz400543f | ACS Macro Lett. 2014, 3, 185−190

the result of adjustments in the ice crystallization rate. Hence, tailoring the geometry and material of the freezing substrate to achieve finer control of cooling rate may allow further opportunities to tune the freeze-dried structure. To investigate this, the CNF/water suspension was frozen at −20 °C using an indented stainless-steel mold that is considerably thicker than the aluminum dishes used above (schematic in Figure S2, Supporting Information). In Figure 5a and 5b, we observe that

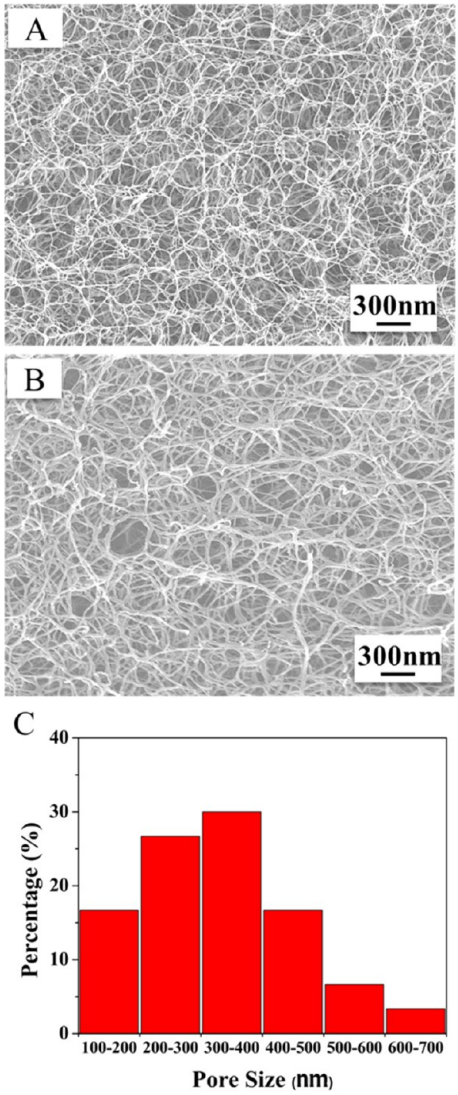

Figure 5. SEM images of chitin freeze-dried using indented stainless-steel mold: (a) bottom, (b) cross section in touch with stainless steel wall; and (c) pore size distribution of freeze-dried chitin under −20 °C freezing (stainless-steel mold).

the resulting freeze-dried chitin is comprised of a fibrous network structure with an average pore size of 326 nm (pore size distribution listed in Figure 5c) and filament diameter near 40 nm, much smaller than the dimensions of chitin frozen in the aluminum dish at −20 °C. The porosity of the structures produced at −20 °C in the stainless-steel mold was 99.6%, compared to 98.5% for the aluminum dish, which is consistent with the finer structures observed in the stainless-steel system. Supercritical drying and organic solvent-based freeze-drying have been shown to produce such finely porous materials previously,[13,38] but it is very rare that this fine structure can be achieved directly by water-based freeze-drying because ice fronts usually advance so quickly that solute or dispersed solids are expelled to form large aggregates. Compared with −20 °C freezing in the aluminum pans, we expect a slowing in ice growth rate in the steel mold due to lower heat transfer rate. The conductive resistance of the steel substrate wall is about 1000 times larger than that of the aluminum substrate ($R_{alum} = \Delta x/k_{alum}$ = 0.2 mm/229 W·(m·K)$^{-1}$ = 8.7 × 10^{-7} (m^2·K)/W versus $R_{steel} = \Delta x/k_{steel}$ = 14.2 mm/16 W·(m·K)$^{-1}$ = 8.9 × 10^{-4} (m^2·K)/W, where Δx = thickness and k = thermal conductivity).[39] The further decrease in the fiber size and pore size is consistent with the model proposed above since the slower moving ice front (steel substrate) exerts less shearing force on the CNF network structure (compared to an aluminum substrate), allowing preservation of finer structures that form early in the CNF aggregation process.

In summary, we have produced the first porous nanofibrous materials derived solely from chitin nanofibers by using a facile freeze-drying method. These structures mimic the size and interconnectivity of the white *Cyphochilus* beetle cuticle but with improved porosity well beyond that of the natural structure (30% to >95%). The formation of such fine nanofibrous structures is not predicted by the widely used particle encapsulation model and has not been demonstrated previously using freeze-drying. We reason that the nanofibrous network structure is made possible because chitin nanofibers are insoluble, and they experience significant attractive interactions. Combined with a slow freezing rate, the network structure remains intact during freezing. We have shown that versatile porous structures can be achieved by simply adjusting freezing temperature or system geometry. Previously, supercritical drying and organic solvent-based freeze-drying have been used to generate delicately porous fibrous materials because water-based freeze-drying usually results in significant aggregations of original building blocks. In contrast, our findings show how to achieve such fine structures by more facile water-based freeze-drying. The innovative, sustainably sourced chitin materials are of ideal size range to be useful in a wide variety of applications, including as components of thermal insulation, reflective energy-efficient exterior coatings, reinforcing phase for polymer composites, and a basic template for sensors, tissue scaffolds, catalyst supports, filtration, absorbents, and energy storage materials.[6−15,40] The freeze-drying method outlined here should be applicable to tunable assembly of nanofibrous structures from other network-forming water-dispersible polymers and other materials.

■ ASSOCIATED CONTENT

Ⓢ Supporting Information

Experimental section, SEM image of a chitin nanofiber fabricated via fibrillation of purified chitin by high shear homogenization, and a schematic of stainless-steel mold used for −20 °C freezing of chitin nanofibers. This material is available free of charge via the Internet at http://pubs.acs.org.

■ AUTHOR INFORMATION

Corresponding Author

*E-mail: carson.meredith@chbe.gatech.edu.

Notes

The authors declare no competing financial interest.

■ ACKNOWLEDGMENTS

We would like to thank the Institute of Paper Science and Technology (Georgia Institute of Technology) and the Air Force Office of Scientific Research (Grant # FA9550-10-1-0555) for financial support of this research.

■ REFERENCES

(1) Rinaudo, M. *Prog. Polym. Sci.* **2006**, *31*, 603−632.
(2) Pillai, C. K. S.; Paul, W.; Sharma, C. P. *Prog. Polym. Sci.* **2009**, *34*, 641−678.
(3) Nair, K. G.; Dufresne, A. *Biomacromolecules* **2003**, *4*, 657−665.
(4) Raabe, D.; Sachs, C.; Romano, P. *Acta Mater.* **2005**, *53*, 4281−4292.
(5) Vukusic, P.; Hallam, B.; Noyes, J. *Science* **2007**, *315*, 348−348.
(6) Ye, C.; Li, M.; Hu, J.; Cheng, Q.; Jiang, L.; Song, Y. *Energy Environ. Sci.* **2011**, *4*, 3364−3367.
(7) Ng, R.; Zang, R.; Yang, K. K.; Liu, N.; Yang, S. T. *R. Soc. Chem. Adv.* **2012**, *2*, 10110−10124.
(8) La Torre, A.; Gimenez-Lopez, M. d. C.; Fay, M. W.; Rance, G. A.; Solomonsz, W. A.; Chamberlain, T. W.; Brown, P. D.; Khlobystov, A. N. *ACS Nano* **2012**, *6*, 2000−2007.
(9) Korhonen, J. T.; Hiekkataipale, P.; Malm, J.; Karppinen, M.; Ikkala, O.; Ras, R. H. A. *ACS Nano* **2011**, *5*, 1967−1974.
(10) Liang, H. W.; Wang, L.; Chen, P. Y.; Lin, H. T.; Chen, L. F.; He, D.; Yu, S. H. *Adv. Mater.* **2010**, *22*, 4691−4695.
(11) Yuan, J.; Liu, X.; Akbulut, O.; Hu, J.; Suib, S. L.; Kong, J.; Stellacci, F. *Nat. Nanotechnol.* **2008**, *3*, 332−336.
(12) Gu, G.; Schmid, M.; Chiu, P. W.; Minett, A.; Fraysse, J.; Kim, G. T.; Roth, S.; Kozlov, M.; Munoz, E.; Baughman, R. H. *Nat. Mater.* **2003**, *2*, 316−319.
(13) Capadona, J. R.; Van Den Berg, O.; Capadona, L. A.; Schroeter, M.; Rowan, S. J.; Tyler, D. J.; Weder, C. *Nat. Nanotechnol.* **2007**, *2*, 765−769.
(14) Chen, L. F.; Zhang, X. D.; Liang, H. W.; Kong, M.; Guan, Q. F.; Chen, P.; Wu, Z. Y.; Yu, S. H. *ACS Nano* **2012**, *6*, 7092−7102.
(15) Qie, L.; Chen, W. M.; Wang, Z. H.; Shao, Q. G.; Li, X.; Yuan, L. X.; Hu, X. L.; Zhang, W. X.; Huang, Y. H. *Adv. Mater.* **2012**, *24*, 2047−2050.
(16) Hartgerink, J. D.; Beniash, E.; Stupp, S. I. *Science* **2001**, *294*, 1684−1688.
(17) Aida, T.; Meijer, E. W.; Stupp, S. I. *Science* **2012**, *335*, 813−817.
(18) Min, B. M.; Lee, S. W.; Lim, J. N.; You, Y.; Lee, T. S.; Kang, P. H.; Park, W. H. *Polymer* **2004**, *45*, 7137−7142.
(19) Madihally, S. V.; Matthew, H. W. T. *Biomaterials* **1999**, *20*, 1133−1142.
(20) Qian, L.; Zhang, H. *Green Chem.* **2010**, *12*, 1207−1214.
(21) Munch, E.; Launey, M. E.; Alsem, D. H.; Saiz, E.; Tomsia, A. P.; Ritchie, R. O. *Science* **2008**, *322*, 1516−1520.
(22) Gutierrez, M. C.; Ferrer, M. L.; del Monte, F. *Chem. Mater.* **2008**, *20*, 634−648.
(23) Deville, S.; Saiz, E.; Nalla, R. K.; Tomsia, A. P. *Science* **2006**, *311*, 515−518.
(24) Zhang, H. F.; Hussain, I.; Brust, M.; Butler, M. F.; Rannard, S. P.; Cooper, A. I. *Nat. Mater.* **2005**, *4*, 787−793.
(25) Xu, Z.; Zhang, Y.; Li, P. G.; Gao, C. *ACS Nano* **2012**, *6*, 7103−7113.
(26) Deville, S. *Adv. Eng. Mater.* **2008**, *10*, 155−169.
(27) Yan, J.; Chen, Z.; Jiang, J.; Tan, L.; Zeng, X. C. *Adv. Mater.* **2009**, *21*, 314−319.
(28) Koehnke, T.; Lin, A.; Elder, T.; Theliander, H.; Ragauskas, A. J. *Green Chem.* **2012**, *14*, 1864−1869.
(29) Petzold, G.; Aguilera, J. M. *Food Biophys.* **2009**, *4*, 378−396.
(30) Kiani, H.; Sun, D. W. *Trends Food Sci. Technol.* **2011**, *22*, 407−426.
(31) Hobbs, P. V. *Ice Physics*; Clarendon Press: Oxford, 1974.
(32) Korber, C.; Rau, G.; Cosman, M. D.; Cravalho, E. G. *J. Cryst. Growth* **1985**, *72*, 649−662.
(33) Wegst, U. G. K.; Schecter, M.; Donius, A. E.; Hunger, P. M. *Phil. Trans. R. Soc. A* **2010**, *368*, 2099−2121.
(34) Rodrigues, M. A.; Miller, M. A.; Glass, M. A.; Singh, S. K.; Johnston, K. P. *J. Pharm. Sci.* **2011**, *100*, 1316−1329.
(35) Gutierrez, M. C.; Garcia-Carvajal, Z. Y.; Jobbagy, M.; Rubio, T.; Yuste, L.; Rojo, F.; Ferrer, M. L.; del Monte, F. *Adv. Funct. Mater.* **2007**, *17*, 3505−3513.
(36) Svagan, A. J.; Jensen, P.; Dvinskikh, S. V.; Furo, I.; Berglund, L. A. *J. Mater. Chem.* **2010**, *20*, 6646−6654.
(37) Tzoumaki, M. V.; Moschakis, T.; Biliaderis, C. G. *Biomacromolecules* **2010**, *11*, 175−181.
(38) Nogi, M.; Kurosaki, F.; Yano, H.; Takano, M. *Carbohydr. Polym.* **2010**, *81*, 919−924.
(39) Welty, J. R.; Wicks, C. E.; Wilson, R. E.; Rorrer, G. *Fundamentals of Momentum, Heat, and Mass Transfer*; Wiley: Oregon, USA, 2001.
(40) Clyne, T. W.; Golosnoy, I. O.; Tan, J. C.; Markaki, A. E. *Phil. Trans. R. Soc. A* **2006**, *364*, 125−146.